Article

Distribution of Uranium and Rare Elements in Radioactive Phosphate-Bearing Anomalies in Southeast Mongolia

Boris Vakanjac [1], Neil Rutherford [2], Vesna Ristić Vakanjac [3],*, Tanita Đumić [1] and Suzana Đorđević Milošević [1]

[1] Faculty of Sustainable Development and Environment, Singidunum University, 11000 Belgrade, Serbia; bvakanjac@singidunum.ac.rs (B.V.); tanitadj@gmail.com (T.Đ.); sdjordjevicmilosevic@singidunum.ac.rs (S.Đ.M.)

[2] Rutherford Mineral Resource Consultants, Coogee NSW 2034, Australia; email@rminres.com.au

[3] Faculty of Mining and Geology, University of Belgrade, 11000 Belgrade, Serbia

* Correspondence: vesna.ristic@rgf.bg.ac.rs

check for updates

Abstract: Soviet and Mongolian geologists initiated geological exploration of Mongolia for minerals after World War II (1945). These activities lasted until the breakup of the USSR in 1991. As part of this exploration systematic uranium and rare element exploration was undertaken across Mongolia. New exploration resumed in Mongolia at the beginning of the 21st century for a range of ore and mineral deposit styles including uranium, coal, base and precious metals and Fe-ore. This was generally undertaken by Western-based companies. This paper presents the results from regional reassessment by company exploration in 2011 for uranium radiometric anomalism found during the early Soviet investigations located north of Sainshand Provincial City and the results of preliminary prospecting studies near the town of Mandakh, both in southeastern Mongolia. These radioactive sites are characterized by elevated phosphate–uranium-rare element abundance. The primary company exploration objective of the new study was to confirm and characterize the anomalies and investigate in more detail the concentration of uranium and rare elements at these sites and assess the economic potential for their exploitation. A secondary objective based on the results from radiochemistry and rare element content was to highlight the potential environmental impact on livestock pastoral activities and wellbeing of nomadic families who graze their stock over the anomalous zones in the region. The source of most of the anomalism is considered derived from erosion and subsequent transport in solution or in heavy minerals from extensively eroded granites and mafic magmas of various ages into graben basins and drainage depressions in the windswept arid terrain. The economic potential of the sites explored was considered too low to be of exploration interest. The anomalism does require characterization for environmental health and safety purposes, given sheep, goats, camels and other livestock traditionally bred in Mongolia are grazing on the enriched pasture and nomadic people reside on, or in their vicinity of elevated zones of radiometric anomalism from anomalous uranium, radon and radium held in phosphorus enriched soils.

Keywords: uranium; radioactivity; Cretaceous; rare metals; phosphate; anomalies; Dornogovi

1. Introduction

The main aim of the exploration presented in this paper is to define areas, prospective for possible related rare elements (REE) deposits. Phosphate concentrations in desert environments and shallow water sedimentary settings are a recognized mineral resource [1]. These rocks are often radioactive and can carry elevated rare earth and other related rare elements [2,3]. Today more researchers are

exploring this issue. The problem of radioactive phosphate is present because of their utilization as fertilizers [4,5]. That they can also carry rare and radiogenic elements was the reason for the research presented in this paper.

The demand for uranium, rare earth and related rare elements (REE) has increased in recent times to meet new technological requirements and this has increased interest in exploration activity for these elements [6–8]. More than 1100 uranium and radioactive anomalies and ~300 such zones were discovered during earlier Soviet exploration and more recent exploration undertaken by Western companies.

The main aim of the exploration presented in this paper is to define potential areas for possible REE deposit.

The starting point of the 2011 exploration activities discussed in this paper was the Report of the Airborne Geophysical Survey at Scale 1:25,000 carried out in the Dorno–Gobi Region [9]. Report documentation consists of a descriptive text, a catalog of anomalies and six maps:

- Geological map (one map);
- Airborne survey with elements of prognosis map (one map);
- Gamma field, uranium, thorium, and potassium distribution maps (four maps).

  Other reference materials included:

- Evaluation of Uranium Bearing Potential of East Mongolia (Vol 1 and Vol 2) [10];
- Metallogenetic Uranium Map of Eastern Mongolia;
- Radio-geochemical map of Eastern Mongolia, complete with legends.

A company digitized geological map of southern and southeastern Mongolia was generated in 2006/2007 from data contained in the above reports. This was used in the 2011 research program.

The uranium ore potential of southeastern Mongolia was of particular interest because of a specific geologic framework that includes closed horst-graben basin systems and Cretaceous sediment packages from Early Cretaceous (K_1), Hauterivian–Albian, Zuunbayan (K_1dz) to Late Cretaceous (K_2), Cenomanian–Santonian, Bayan Shireh (K_2bs) suites.

In addition, there are recent occurrences associated with surface interface zones between oxidizing and reducing (redox) environments, where the soluble uranyl ion (U(VI)) is reduced and precipitated from solutions during rare rain events, as well as in small salt lakes with deposits of organic material (which often dry out), limonitic sandstones and clays, outcrops of organic-coaly plant matter, and as carbonate–phosphate±(vanadate) precipitates.

A compilation of anomalies and their characteristics from historical maps in MRAM reports (Mineral Resource Authority of Mongolia-MRAM nomenclature) was undertaken. This indicated that over 80 uranium-phosphate bearing anomalies were present. However, this is not a definitive number because metallogenetic and radiogeochemical maps and data from the Eastern Mongolian uranium survey (MRAM Report 2451), show many types of element anomalies, other than those related to phosphates, and give descriptive text explanation and referrals to phosphates in other reports. There are also inconsistencies between the metallogenetic, and radiogeochemical map of MRAM Report 2451 [10] on the anomalies of different genesis, their positions and numbers.

Generally, phosphate anomalies (Figure 1) can be classified in terms of the environments in which they are developed, that is, connected to:

1. Sites where the dominant sediments are usually pebble conglomerate, sandstone and siltstone. Where the clasts are mostly of quartz and granite and rarely feldspar, sericite, and basalt. They are cemented with greater concentrations of phosphate-carbonate cement. These were observed within the K_1 (Hauterivian–Albian) and K_2 (Cenomanian–Santonian) sedimentary series. Some anomalies in this group are associated with limonite occurrences and where limonite is abundant may have increased radioactivity;

2. Coal bearing sedimentary series, in which the upper parts of such occurrences are oxidized and with possible phosphate-containing siltstone layers;

3. Volcanogenic formations, for example, in relation to sediments in the late Jurassic–early Cretaceous volcanic sedimentary series in contact with sedimentary formations (conglomerate, siltstone, sandstone, etc.) with the appearance of Fe-oxides associated with the weathered zone as well as quartz and calcite veins where elevated radioactivity is related to phosphate cement;

4. Hydrothermally altered volcanogenic formations of Early Cretaceous volcano-sediment tectonic blocks made of polymictic sandstone, tuff-sandstone and tuff-siltstone which are intruded by andesite-basalt sill, then fine-grained polymictic sandstone, siltstone, and tuff-sandstone. Andesite–basalt sill is cataclastic, limonitic and phosphatic;

5. Phosphatic appearances in metamorphic rocks, erosion remnants of chlorite–sericite, quartz–sericite schist of late Proterozoic age. Schist is structurally fractured and clay-altered (kaolinite), limonitic, hematitic, silicified and phosphatic.
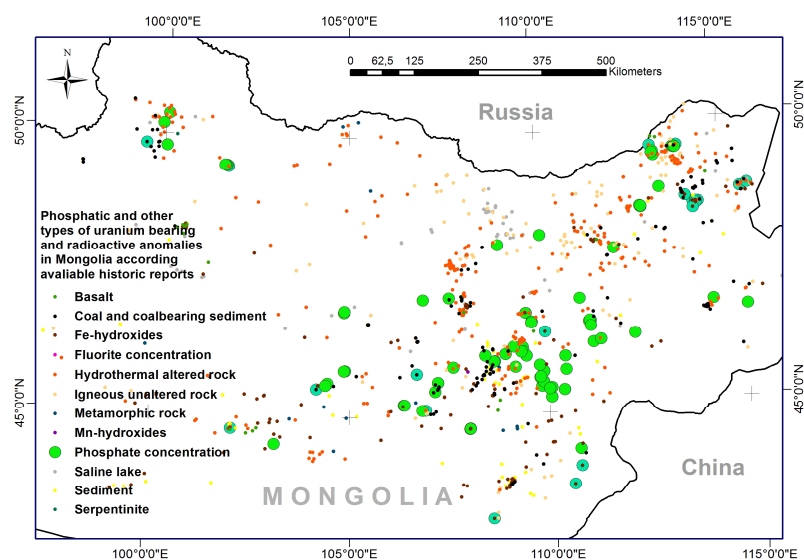

Figure 1. Schematic map of East Mongolia with historical uranium-phosphate bearing anomalies (green dots).

Literature sources [9,10] state that the origin of the natural radioactivity is from uranium, thorium, and potassium (strictly from the radiogenic gamma-ray daughter emitter equivalents of U and Th–^{214}Bi and ^{208}Tl). Background uranium radioactivity flux, as reported in early Russian literature (now redundant units), was 20–22 μrad/h, (1.2–1.4 μSv/h SI equivalent), while in radioactively anomalous areas, uranium radioactivity flux was given as between 85–135 μrad/h (8.7–13.8 μSv/h). It is not possible to directly correlate these values with total gamma count data collected in the field studies discussed here, other than to demonstrate comparable relative levels of anomalism between background and anomaly sites.

In all the selected areas, as well in anomaly areas, uranium concentrations were higher in yellow-white sandstones and terrigenous material. The cement matrix is mainly with uranium carbonated fluorapatite, francolite, podolite, kurskite and monazite. Petrological-chemical tests indicate phosphorus levels of 1%–3% in the uranium haloes. Historical trenches excavated at sites of anomalies 2426/262, 2426/268 and 2426/270 (Figure 2a) exposed lenses and nests of phosphatized sandstones with 100 to 150 ppm uranium-values of U are from historical (Soviet) chemical assay [9–12].

It is considered that the anomalies originated through infiltration processes and deposition of materials within the Upper Cretaceous sediments. Carbonate–phosphate compounds are known to be readily soluble in carbonic acid-rich waters and then can enrich by changes in redox or by evaporation and precipitation by reaction with oxy-anions.
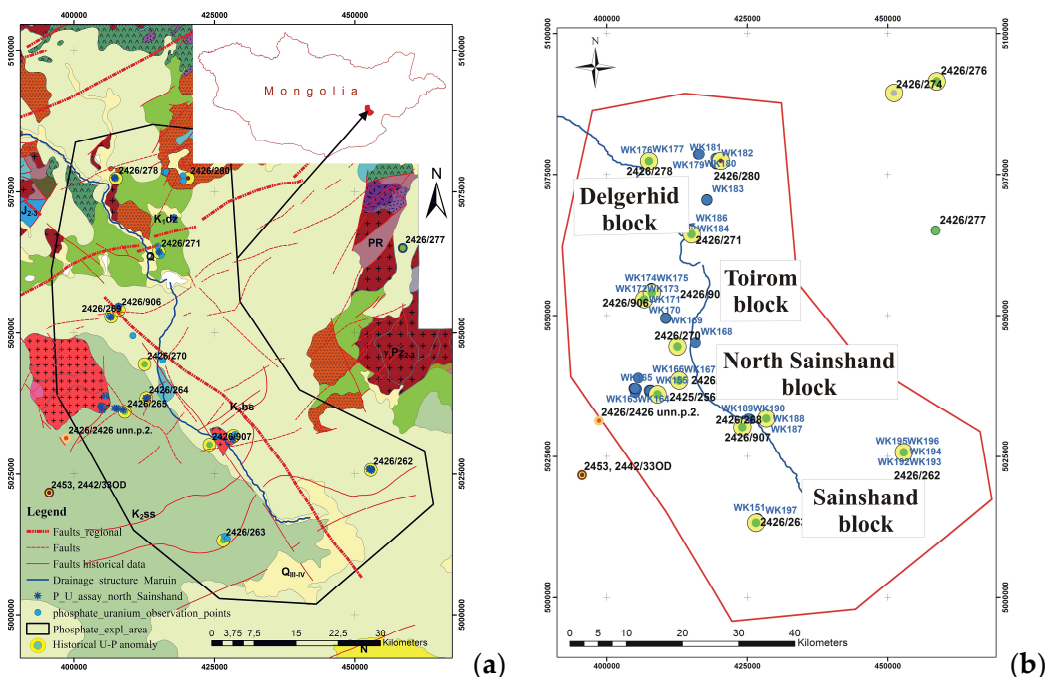
Figure 2. Map of the explored area: (**a**) geological map: granites are red (Mesozoic light red and Paleozoic dark red), Late Jurassic/Early Cretaceous volcanics are orange and Cretaceous sediments are in shades of green. White are areas of salty lakes that are dry in summer. The blue line is the drainage system; (**b**) observation points, historical anomalies—yellow circles with green dots. Blue dots are observation points from recent exploration. Black line polygon is a boundary of the area of interest.

According to Jerden (2001) [13] U(VI) phosphates of the meta-autunite group are not stable in the vadose zone (soil pH ~4.5) at the Coles Hill site. In this zone, uranium is associated with (Ba, Ca, Sr) aluminum phosphate of the crandallite group as well as with phosphate adsorbed onto iron oxy-hydroxide mineral coatings. Uranium leached from the vadose zone is reprecipitated as new meta-autunite minerals below the water table due to higher pH conditions of ~6.0 and relatively high activity ratios of dissolved phosphate to carbonate (e.g., log ($H_2PO_4^-$/HCO_3^-) > −3).

It is estimated that the U(VI) phosphates responsible for the natural enrichment of uranium at this site persist within the weathering zone for hundreds of thousands of years.

2. Methodology

Geochemical prospecting was undertaken on known sites of historic phosphate-bearing anomalies north of Sainshand, within depressions and their peripheral structures, to assess their U-REE resource potential. Historic data from MRAM Report Nos. 2426 and 2451 [9,10] was used.

In general, the uranium concentrations at the explored sites were found to be relatively low–up to 200 ppm as determined by a Thermo Fisher Scientific Niton xl3t (Thermo Scientific, Boston, MA, USA), field-portable XRF (fpXRF) and up to 129 ppm by ICP-MS using a total digest chemical analysis.

The Niton fpXRF was configured for heavy element assay; count integration times were 60 s; instrument calibration was pre-field on assayed pulp calibration standards supplied by ActLabs Mongolia. Field sample preparation methodology was confined to the measurement of sample material collected from sample site holes held within cotton cloth sample bags. High field accuracy was not required at this preliminary stage of the investigation. Measurements were used to determine the magnitude of anomalous elements present, with the objective of selecting anomalous samples to transport for accurate laboratory chemical analysis. A combination of instrumental neutron activation analysis (INAA) and TD-MS method ICP-MS—total 4-acid digest were used for chemical analyses and undertaken at Actlabs and laboratory facilities in Canada.

The maximum radioactive gamma count readings were relatively high, up to almost 1500 cps. The terms radioactive count or radioactivity in the text refers to total gamma count as counts per second (cps) measured in the field using a Handheld Gamma-Ray Spectrometer RS125 (Daxan Ltd., Hertfordshire, UK).

The results of our new investigations and historic exploration generally concur, regarding locations of elevated radioactivity and phosphate-carbonate origin. However, the analyzed concentrations of the tested elements vary from the radiometric determinations of equivalent uranium values (eUppm values) suggesting, often significant, radiometric disequilibrium between radiogenic daughter elements. Estimates of uranium content from uranium channel radiometric count data is therefore quite unreliable but can give a broad guide to the relative difference between sites. Note: equivalent uranium is expressed as eU.

All the studied anomalies were either shallowly buried or in some locations were exposed in historic trench excavations. In some instances, radiometric count readings were higher than 800 cps. There were temporary nomadic stock herder settlements in the local vicinity of anomalies at some locations.

There were three types of anomaly sites identified trending north to south through the area and selected for investigation from the Occurrences Map (Report 2451 [10]):

1. Ten investigated sites: Anomaly points with apatite–pitchblende–uranium–phosphate bearing terrigenous carbonate rocks, sedimentary-diagenesis origin;
2. One investigated site: Uranium in multicolored and grey rocks related to infiltration and water migration, pitchblende–kerite–coffinite;
3. One investigated site: Uranium in multicolored and grey rocks related with soil and sediment layers variable redox zonation, pitchblende–coffinite–selenium.

The exploration methodology included:

1. Checking the potential area with a hand spectrometer (RS 125), limit 250–300 cps or more, on the surface (Figure 2b);
2. Establishing observation points, sampling, and mapping of the area (Figure 2);
3. Checking for phosphate with nitric acid and ammonium molybdate solution (standard field test- sample turns yellow if phosphates are present), these two chemicals are spilled in small quantities on sample;
4. Sampling (soil and rock chips), soil-friable samples were taken with shovel from the depth of 20–50 cm, and rock chip samples were peices of rock, both in amount of 2 kg approximately, and kept in cotton bags; and
5. Field analyses were carried out by fpXRF and chemical analysis by ICP-MS.

3. Explored Area

The twelve anomalies, to the north of the provincial capital, Sainshand. Multiple uranium anomalies were detected in this area by historic aerial gamma spectrometry. Based on historic records of phosphate in MRAM Report 2426 [9], the following anomalies, numbered 263, 262, 907, 268, 265, 264, 270, 269, 906, 271, 278 and 280 and shown in Figure 2 were considered of sufficient merit for further exploration. These were also shown in MRAM Report 2451 and on the metallogenic and radiochemical maps of eastern Mongolia. The anomalies are contained within an area of about 70×9–25 km.

Company field exploration indicated that the size of some zones of elevated radioactivity encompassed several square kilometers. The criteria were morphological (whether it was depression) and geological (whether built up of Late Cretaceous K_2ss and K_2bs, Cenomanian to Santonian, or younger sedimentary formations).

The surrounding geology of the Sainshand and Delgerhid valleys includes various intrusive, metamorphic, effusive and sedimentary rocks. These are Early–Middle Paleozoic gneiss, granite–gneiss,

crystalline schist, marble and amphibolite, Early Paleozoic granitoids, Middle–Late Paleozoic granites and granodiorites, Late Jurassic conglomerate, sandstone, and andesite–basalt, as well as Late Jurassic/Early Cretaceous volcanics and complexes of pyroclastic rocks.

Ulaan-nuur north, Caganudin, and Shinebulgin are packages within horsts composed of Paleozoic metamorphic rocks and granites, which overlie Late Jurassic to Early Cretaceous sediments and igneous rocks. They are interconnected in narrow zones, except for the Shinebulgin valley that is built up of K_2bs sediments developed in Late Jurassic/Early Cretaceous andesites and andesite-basalts and Early Cretaceous basalts.

The field investigations carried out in 2011 revealed that anomalies 268 and 907 were associated with proximity to the Late Triassic/Early Jurassic granites, and anomalies 280 and 278 with an area of Late Jurassic to Early Cretaceous igneous rocks.

There is a distinct drainage system in the explored area, ~50 km long and associated with anomalies 907, 268, 264 and 270.

Ulaan-nuur North, Caganudin and Shinebulgin are contained within restricted depressions within horsts composed of Paleozoic metamorphic rocks and granites, which overlie Late Jurassic to Early Cretaceous sediments and igneous rocks. Except for the Shinebulgin Valley they are interconnected in narrow zones. It is believed that the anomalies originate from infiltration processes and the deposition of material within Late Cretaceous sediments. As stated previously carbonate-phosphate compounds readily transport in carbonic acid-rich water, thereby increasing the concentrations of the anomalies [14].

4. Results and Comments

The distribution of the anomalies in the explored area can be subdivided into four blocks. This can be done in terms of whether they are associated with horst or graben systems and from which geologic constituents the tectonic units are composed. In the accompanying figures designations like 2426/269 are original site identifiers from Soviet reports, and those like WK187 are our designations of the observation points.

Delgerhid Block Anomalies—Horst is not the largest but the most complex geologically. The initial anomalies include sites 2426/278, 2426/280, 2451/65 and 2426/271 (Figure 3a), mostly composed of Late Cretaceous sediments and Late Jurassic to Early Cretaceous volcanics. The geologic framework (Figure 2a) comprises: Middle to Late Paleozoic granites γPz_{2-3} trending at N-S, in contact with the Late Jurassic/Early Cretaceous igneous complex J_3-K_1dz or $\alpha\beta J_3$-K_1, which includes basalt, andesite-basalt, tuff, tuff-sandstone, rhyolite, and tuff lava. The Paleozoic formations and Mesozoic volcanics are in contact with the Early Cretaceous sedimentary series K_1dz, which is recognizable on the ground and generally serves as a reference because of its typical medium-to-coarse conglomerate and sandstone interbeds occurrences of carbonaceous material and local (sometimes intensive) limonitization. Nearby, north of initial anomaly 2426/271, there is the NE-SW Undurshil-Delgerhid regional fault, detected by measuring linear magnetic anomalies [9] associated with outcrops of Mesozoic volcanics.

The initial description was that the anomaly is situated in an area built up of poorly lithified sediments of the Early Cretaceous Dzuunbayan suite, represented by fine-grained pebble conglomerate, limestone, and horizons of sedimentary breccia. The uranium anomaly is related to the breccia horizons, composed of fragments of basalt and quartz cemented with uranium-bearing phosphate clay. According to the Soviet radio geochemical map in Report 2451 [10], the anomaly is situated on the edge of a granite intrusion in contact with K_1dz on the south side and K_2bs on the north side of the anomaly.

Based on our exploration, the anomaly is located within a system of salt lakes/wetlands, whose water depth varied over the seasons and years. Light and dark shades were clearly visible on the ground and there was little or no grass on the light surfaces. The area of surface deposits created by frequent flooding and drying is about 10 × 5 km. An orthophoto clearly showed these as lighter coloured clusters of deposits originating from cyclical drying. The zone of elevated radioactivity, shown in the Soviet airborne survey, indicated a coherent anomaly of 3–4 ppm eU values determined from radium analysis and 7 × 5 km in extent). Within it, three sub-zones in the lake/wetland area,

whose average size was 600 × 600 to 1000 m with 4–5 ppm eU values determined from radium analysis. The explored area was covered by gravelly and clayey material, with varying amounts of chalcedony that was always gel-like and in shades of grayish-white to white. The cement was carbonate clay.

| (**a**) | (**b**) |

Figure 3. (**a**) Sample of the Delgerhid block, anomaly 2426/271; (**b**) sample of the Sainshand block, from Soviet excavation, anomaly 2426/262.

There was a dark brown interbed variably at 10, 20, and 30 cm depth from the ground surface and additional interbeds at a depth of 30–40 cm, which was lighter in color and with increasing radioactivity. Their thickness varied, up to several tens of cm. Fragments cemented with clayey carbonate material were slightly rounded and their size was generally from several mm to 1 cm. There was a poorly lithified conglomerate, mainly composed of quartz and feldspar, with local basalt fragments. The hand spectrometer measured radioactivity from 570 to 620 cps and uranium grade from 25 to 45 ppm. The thorium grade was from 8 to 15 ppm. The uranium grade measured by Niton fpXRF, varied from 38 to 165 ppm and based on ActLab ICP-MS chemical assays it was 56 to 129 ppm. Thorium was below 10 ppm. The phosphate test was negative and P was very low, around 0.04% from ActLab chemical assays.

Historically, the anomaly was described as erosional outliers of Early Cretaceous sandstone, sedimentary breccia, and conglomerate that overlie Late/Early Cretaceous basalt. The radioactivity was associated with outcrops of breccias and sandstones. The sandstones are whitened and show signs of limonitization. Our exploration revealed two groups of anomalies on the initial historical position.

The first group of anomalies were at 4 km approximately from the initial anomaly and associated with fine-grained (along poorly limonitic fractures) andesite-basalt tuff and whitened (along with highly limonitic fractures) tuff-siltstone. There the Fe-oxide concentrations were higher than those of all the other samples. In the sample that measured 77,820 ppm (7.78%) Fe (Niton fpXRF), uranium and thorium were below the detection level. This group also exhibited the highest concentrations of Mn, Zn (111 ppm) and Pb (22 ppm), in samples where U and Th were also below the detection level. Radioactivity ranged from 310 to 350 cps but was absent in the basalt outcrops. Elevated radioactivity was associated with whitened and limonitic tuff-siltstone. The phosphate tests of both igneous products were negative.

The second group of anomalies were at ~1 km from the initial anomaly. They were composed of friable whitish sediments and conglomerates with siltstone cement, moderately limonitic. Signs of drying were noticeable. There was a wetland and a salt lake in the vicinity. The radioactivity was ~400 cps and the field phosphate test was positive. The uranium grade (Niton fpXRF) was between 25 and 29 ppm. The samples from this group measured Zr concentration up to 288 ppm, like that of the granitic group of rock samples. The orthophoto of the area showed brownish-red shades indicative of the presence of Fe hydroxides originating from weathering of volcanics.

The anomaly on the radio-geochemical map in Report 2451 is shown as phosphatic in ferruginous and carbonaceous sediments. The hand spectrometer readings were 120 cps, associated with whitish

loose pebbles and sandy-clay material. The Niton fpXRF assay indicated that uranium was below the detection limit. The concentration of thorium was 13 ppm. The ActLab assays indicated 3 ppm U and 16 ppm Th. The phosphate test was negative. Historic data indicates the anomalies are developed in Early Cretaceous limestone gravelite and polymictic fine-grained conglomerate, including clay and clay-carbonate cement with phosphates. Our investigations of shallow trench excavations revealed three layers from the ground surface to a depth of 75 cm. The first layer consisted of brownish-gray fine-grained sand (soil) with plant remnants (thickness 10–15 cm), the second layer was light gray to white argillaceous sand, with carbonaceous particles and fine-grained fragments (the radioactivity was elevated), and the third layer was dark to light gray argillaceous clayey sand. The radioactivity of the second layer was 537 cps, the uranium grade was from 20 to 22 ppm and the thorium grade from 7 to 13 ppm (Niton fpXRF). The ActLab assays showed 26 ppm of U and 6ppm of Th.

Toirom Block Anomalies—Graben, with initial anomalies 2426/906, 2426/269 and 2426/270. These anomalies are composed of the Late Cretaceous Bayan Shireh suite (K_2bs). The southern extension of the Choyren regional fault runs through them (NNW-SSE).

The anomalies are in Late Cretaceous K_2ss sediments, composed of well-bedded poorly lithified conglomerates and polymictic sandstones with phosphatic clay cement. The concentration of uranium was 66 ppm and of thorium 5 ppm (Niton fpXRF). Our exploration revealed that the anomaly was in medium-grained carbonaceous sandstone and conglomerate with loose pebbles. The phosphate test was positive. Shallow excavations showed two layers: (i) upper, 40 cm thick and composed of sand, gravel and brown clay, and (ii) lower, below a depth of 40–70 cm, built up of sand and gravel, cemented or with white carbonaceous phosphate-bearing material. The radioactivity measured with the hand spectrometer was high, 1377 to 1495 cps, the Niton fpXRF uranium grade was from 64 to 95 ppm, and the thorium grade up to 11 ppm. ActLab assays indicated a uranium grade of 41 to 63 ppm and a thorium grade from 5 to 9 ppm.

Anomalies of the North Sainshand Block—Horst, with initial anomalies 2426/264, 2426/265, 2426/268 and 2426/907, comprised of outcrops of granite, granodiorite, and granosyenite (γPz_{2-3}) according to Report 2451 [10], and leucocratic, biotitic and alkaline granites and rare granosyenite, syenite and porphyritic granosyenite (γT_3-J_1). In addition to granites, there were outcrops of conglomerate, sandstone, tuff-sandstone, siltstone, schist, coal-schist and rarely rhyolite. The observed area was an outcrop of granite (batholith), light yellowish gray, medium-grained, weakly leached and oxidized, with Fe hydroxides in fractures. The sedimentary formations were the Late Cretaceous/Sainshand suite and Neogene. The highest radioactivity reading was 500 cps but the uranium grade was relatively low (2.5 to 3.5 ppm, maximum 40 ppm—Niton fpXRF) at the point of contact with the sedimentary formations. A little to the south there was also a granite outcrop, which was likely the source of the radioactivity of initial anomalies 268 and 907, where the uranium grade was 182 ppm.

Anomalies of the Sainshand Block—Including initial anomalies 2426/263 and 2426/262 is composed of the Cenomanian K_2ss (Sainshand) suite and Cenomanian/Santonian K_2bs Bayan Shireh suite. In this area, there were several Soviet trench excavations, whose length was 60 m and width 4–5 m. The soil sampling hole consisted of three layers, including (i) brown fine-grained sand (soil), thickness 15–20 cm, radioactivity 300–350 cps; (ii) light gray to white medium-grained carbonaceous sandstone with phosphate, thickness 10 cm, and radioactivity 934 cps; and (iii) dark brown medium-grained sand with radioactivity of 450–500 cps. There were also other excavations, several decades old. In one instance, the radioactivity reading was as high as 1200 cps (outcrop shown in Figure 3b).

In order to identify the explored anomalies, samples were analyzed for 17 elements by ActLabs (Ba, K, Li, P, Rb, Sc, Sr, Th, U, V, Y, La, Ce, Nd, Sm, Yb, and Lu). A summary of their characteristics is provided below. On Figures 4 and 5 are given bar diagrams of elements of interest. It should be noted that the samples were collected from topsoil (up to 50cm) and then compared accordingly.
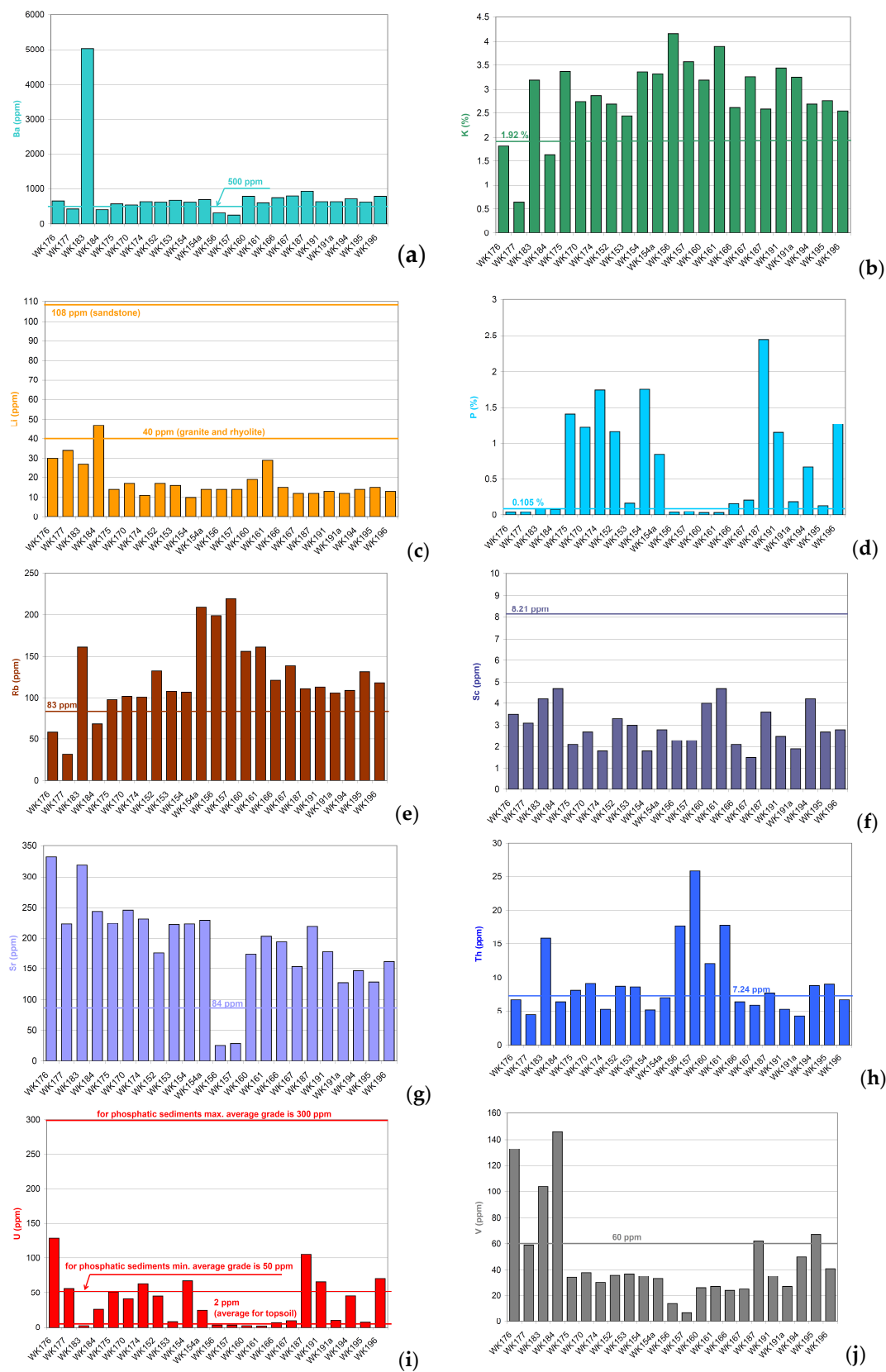
Figure 4. Graphics of grades (**a**) barium—Ba, (**b**) potassium—K, (**c**) lithium—Li, (**d**) phosphorus—P, (**e**) rubidium—Rb, (**f**) scandium—Sc, (**g**) strontium—Sr, (**h**) thorium—Th, (**i**) uranium—U, (**j**) vanadium—V.
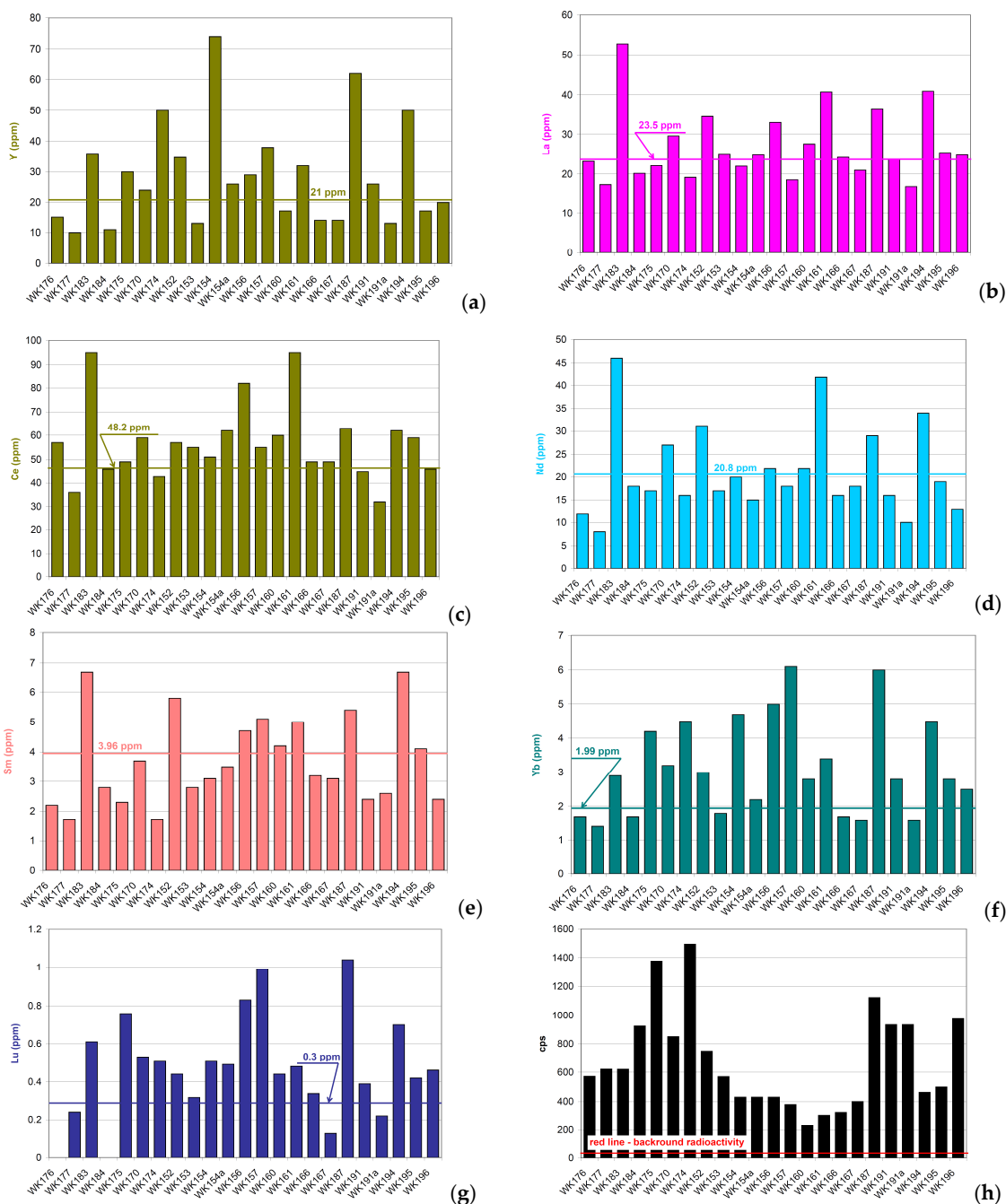
Figure 5. Graphics of grades (**a**) yttrium—Y, (**b**) lanthanum—La, (**c**) cerium—Ce, (**d**) neodymium—Nd, (**e**) samarium—Sm, (**f**) ytterbium—Yb, (**g**) lutetium—Lu and (**h**) radioactivity in counts/sec (cps).

The highest concentration of barium (Ba) was measured at point WK183 (Table 1), Delgerhid block, at the contact between Quaternary and Lower Cretaceous sediments. The concentration was 5040 ppm (Figure 4a) and the sample was a light grayish-brown carbonaceous conglomerate with loose pebbles (Figure 6a). The radioactivity was 620 cps. The average concentration in Regional European Studies (RES) in soil is 500 ppm [15].

Table 1. The highest values determined from sample points and areas.

| Element	Maximum Value	Sample Point	Historic Point	Geology	Block
U	129 ppm	WK176	2426/278	Quaternary cover In vicinity on Paleozoic granite γPz_{2-3}	Delgerhid block
Nd	46 ppm	WK183	2426/271	Early Cretaceous $K_1 dz$ sediments	
La	53 ppm				
Sm	7 ppm				
Ce	95 ppm				
Ba	5040 ppm				
Li	47 ppm	WK184	2426/271	Early Cretaceous $K_1 dz$ sediments	
V	146 ppm				
P	2.44%	WK187	2426/265	Cretaceous sediments($K_2 ss$) in vicinity of granite outcrop Late Triassic—Early Jurassic age	North Sainshand block
Lu	1 ppm	WK157	2426/265	Cretaceous $K_2 ss$ sediments	
Rb	220 ppm				
Yb	6 ppm				
Th	25 ppm				
Ce	95 ppm	WK161	2426/265	Granite outcrop Late Triassic—Early Jurassic age $\gamma_2 T_3 J_1 b$	
K	4.16 %	WK156	2426/265	Granite outcrop Late Triassic—Early Jurassic age $\gamma_2 T_3 J_1 b$	
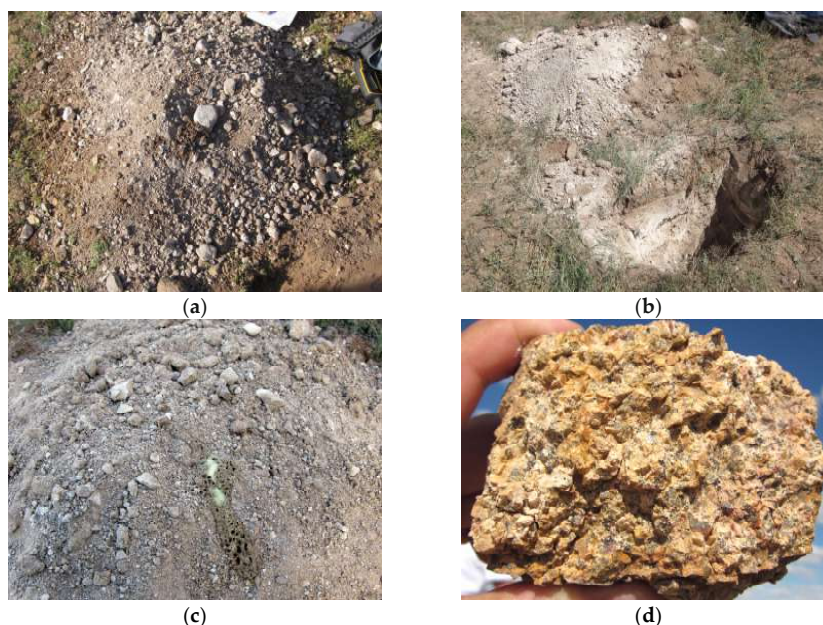
Figure 6. (**a**) WK183 light grayish-brown carbonaceous conglomerate with loose pebbles; (**b**) WK184 brownish-gray fine-grained sand, whitish-gray siltstone and dark to light gray siltstone; (**c**) WK161 brown sand with granite fragments clasts; yellow in the center is the reaction of nitric acid and ammonium molybdate with phosphorus in the sample; (**d**) WK157 coarse-grained granite, Late Triassic—Early Jurassic age.

Potassium (K)—Its highest concentration was measured at point WK156, North Sainshand block, where it assayed up to 4.16% (Figure 4b). This is more than double the average for topsoil in RES, which is 1.92% [16,17]). The sample was collected in area of contact of Upper Triassic/Lower Jurassic granite and Cretaceous (K$_2$bs) sediments. The radioactivity was 430 cps.

Lithium (Li)—The highest concentration of lithium was measured at point WK184 (Figure 6b), (Table 1), Delgerhid block, at the contact between Quaternary and Early Cretaceous sediments, where it amounted to 47 ppm (Figure 4c). This is low compared to maximum concentrations in sandstone reported in RES where, in granite and rhyolite, Li is present in concentrations of 30–70 ppm (average 40 ppm) and in sandstone 0.5–216 ppm [16,17]. The sample was brownish-gray fine-grained sand, whitish-gray siltstone and dark- to light-gray siltstone. The radioactivity was 924 cps.

Elemental phosphorus (P)—The highest concentration was measured at point WK187 (Table 1) (Figure 4d); North Sainshand block, in Cretaceous sediments (K$_2$ss), 1.6 km east of an Upper Triassic/Lower Jurassic granite formation, in Delgerhid block. The concentration of P was 2.44%, (average grade for P in sandstone in RES is 170 ppm; and in carbonate rocks, 400 ppm [16,17], average abundance in Earth's crust is 1050 ppm [18]). The sample was light gray medium-grained pebble conglomerate with sand. Its radioactivity was 430 cps.

Rubidium (Rb)—The highest concentration was measured at point WK157, North Sainshand block, in Cretaceous sediments (K$_2$ss). It was 220 ppm of Rb (Figure 4e), which is much higher than the topsoil average in RES of 83 ppm [16,17]). The sample was whitish-gray carbonaceous sandstone with loose pebbles. Its radioactivity was 380 cps.

Scandium (Sc)—The highest concentrations were measured at points WK161 (Table 1) (Figure 4f) and WK184, where they amount to 5 ppm, which is very low. The average RES concentration [16,17] in topsoil is 8 ppm. The radioactivity was 300 and 924 cps, respectively. Sample WK184 is described above with Li. Sample WK161 was brown sand with granite fragments (Figure 6c), of Late Triassic/Early Jurassic age, in the north Sainshand block.

Strontium (Sr)—The average amount of strontium found in RES topsoil is 84 ppm [16,17]. The highest concentration was measured at point WK176 (Figure 4g), Delgerhid block, in Quaternary sediments, near Paleozoic granites, where it was 332 ppm of Sr—four times higher than average. The sample was whitish-gray carbonaceous clay with chalcedony. Its radioactivity was 572 cps.

Thorium (Th)—The average RES concentration [16,17] in topsoil is 7 ppm and the range is 0.3–75 ppm, depending on the parent rock. The highest concentration was measured at point WK157 (Table 1) (Figure 4h), North Sainshand block, in Upper Triassic/Lower Jurassic granite, where Th was 26 ppm—three times higher than average. The sample was light brownish-gray coarse-grained granite, with thin Fe hydroxide stains along fractures. Its radioactivity was 380 cps (Figure 6d).

Uranium (U)—The highest concentration was measured at point WK176, where it was 129 ppm (Figure 4i)– above average and beyond the RES topsoil range, but still almost half of what might be expected in phosphatic sediments. The average RES concentration of U in topsoil is 2 ppm and the range is 0.2–53 ppm, depending on the parent rock and 50–300 pm in phosphatic sediments [16,17]. The sample is described above with strontium. Its radioactivity was 572 cps.

Vanadium (V)—The average RES concentration [16,17] in topsoil is 60 ppm and the range is 3–537 ppm, depending on the parent rock. The highest concentration was measured at point WK184 (Figure 4j), where it was 146 ppm—higher than average. The sample is described above with lithium. Its radioactivity was 924 cps.

Yttrium (Y)—The average RES concentration [16,17] in topsoil is 21 ppm and the range is <3–267 ppm, depending on the parent rock. The highest concentration was measured at point WK154 (Figure 5a), North Sainshand block, where it was 74 ppm—higher than average. The sample is described above with phosphorus. Its radioactivity was 430 cps.

Lanthanum (La)—The average RES concentration [16,17] in topsoil is 23 ppm and the range is 1–143 ppm, depending on the parent rock. The highest concentration was measured at point WK183

(Figure 5b), and it reported as 53 ppm—above average. The sample is described above with a barium. Its radioactivity was 620 cps.

Cerium (Ce)—In topsoil, the average RES concentration is 48 ppm with a range of 2–267 ppm, depending on the parent rock [16,17]. The highest concentration was measured at points WK183 (Figure 5c) and WK161, where it reached 95 ppm—above average. The samples are described above with barium (WK183) and scandium (WK161). The radioactivity was 620 and 300 cps, respectively.

Neodymium (Nd)—The average RES concentration [16,17] in topsoil is 20 ppm and a range of 1–132 ppm, depending on the parent rock. The highest concentration was measured at point WK183 (Figure 5d), where it amounted to 46 ppm—above average. The sample is described above in connection with barium. Its radioactivity was 620 cps.

Samarium (Sm)—Its average RES concentration in topsoil is 4 ppm and its range is 0.2–30 ppm, depending on the parent source rock [16,17]. The highest concentration was measured atpoints WK183 (described above with Ba) and WK194 (Figure 5e), Sainshand block, where it amounted to 7 ppm—above average. Sample WK194 was collected 150 m south of an old Soviet exploration trench. It was a brown conglomerate, pebble and sand and whitish gray carbonaceous sand with siltstone. The radioactivity was 620 and 462 cps, respectively.

Ytterbium (Yb)—Its average RES concentration in topsoil is 2 ppm and the range, depending on the parent rock [16,17], is 0.1–25 ppm. The highest concentration was measured at point WK157 (Figure 5f), where it amounted to 6 ppm—above average. The sample is described above in relation to thorium. Its radioactivity was 380 cps.

Lutetium (Lu)—Its average RES concentration [16,17] in topsoil is 0.3 ppm and the range is <0.02–3ppm, depending on the parent rock. The highest concentration was measured at point WK187 (Figure 5g), where it amounted to 1 ppm—above average. The sample is described above in connection with thorium. Its radioactivity was 1123 cps.

The highest count value or gamma radioactivity was measured in sample WK174 (1495 cps) in late Cretaceous K_2bs sediments, composed of sand and gravel, cemented, or with friable white carbonaceous phosphate-bearing material in vicinity of Paleozoic granite (Figure 5h).

Figures 4 and 5 summarize the analytical and radiometric count data from the regional soil sampling program as histograms of maximum site values. There is no field spatial connection implied between adjacent value bars shown on each chart. Each bar is independent of the next and the charts simply serve to illustrate the ranges of values determined from the analytical data for the samples. Shown for reference, as a line across each chart, are the average values (not max values) for European (RES) soils for comparative reference purposes. The result ranges are of course principally controlled by the geochemistry and character of the local rock types, the nature of the erosional and depositional regime present, the geomorphology and regional climate.

In addition, a reconnaissance check was carried out on a group of five historical anomalies investigated in the 1980s located 170 kilometers southwest of the central part of the Sainshand zone near Mandakh settlement. These anomalies are numbered MRAM 2455/3833, 2455/3834, 2455/3832, 2455/556 and 2455/3831. Four old exploration trench excavations were located within this area (Figures 7 and 8). The geological structure of the area of interest is similar to that of the Delgerhid block within the Sainshand zone. Anomalies and excavations are at the very border of the K_1dz sediments and Quaternary cover. These outcrops are also surrounded by K_2ss sediments and Paleogene deposits.

Conglomerate with phosphorus-bearing cement, dark gray calcareous composite, light gray to brown coarse-layered phosphatic sandstone, fine-grained phosphatic sand, and yellow-tinged bright gray argillaceous sandy siltstone were exposed in the wall of old exploration trench (Figure 8b) and in the field. In some areas, the conglomerate was coarsely bedded. The conglomerate and sandstone were enriched by iron oxide, with hematite veins up to 1 to 2 mm in width. The coarse-layered sandstone was porous and fractured due to elutriation; the bright gray, fine-grained sandstone was less oxidized. The radioactive anomalies occur in a fault zone, finer sandstone, coarse bedded sand, conglomerate, with noticeable U-Th occurring in a 10 m wide zone within the trenches. This extends about 100 m

northward and 200 m to the south, gradually disappearing beneath the Quaternary sediment. Hand spectrometer (RS125) readings were 330 to 1500 cps.
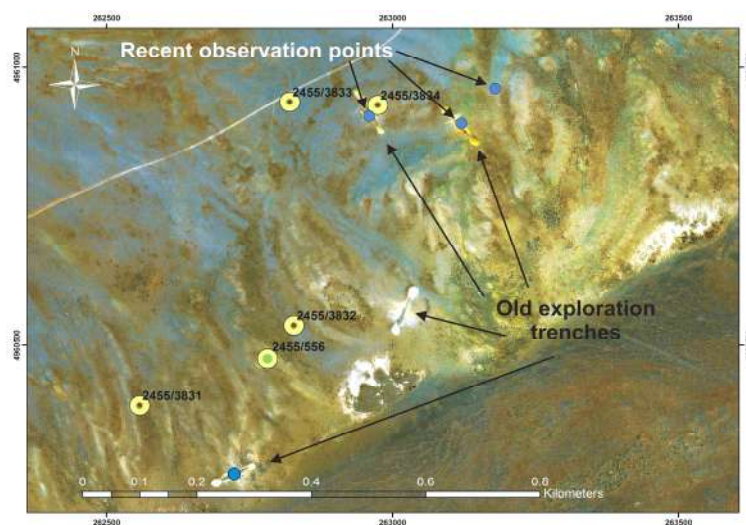

Figure 7. Old exploration trenches and recent observation points in Mandakh area. Raster basis: SASPlanet ESRI ArcGIS Imagery.

| (**a**) | (**b**) |

Figure 8. (**a**) Old Russian trench (dug in 1980). General overview. Conglomerate and sandstone trending to SE; (**b**) Historic exploration trench, the picture is of NE wall of the trench, length of the section marked with a black line is approximately 6 m. 1. Dark gray sandstone, 2. Conglomerate and coarse-grained sandstone bearing phosphate, measured with RS125 spectrometer: U—93 ppm, Th—75 ppm, K—0.8%, radioactivity was 720 cps and 3. Gray phosphatic sandstone.

Uplifted terrain with about 5 m to 10 m undulating surfaces was predominant in the study area. The radiation anomaly continued, with interruptions, to the lower slope of the terrain. The fault continued NE along the terrain slope and split into several sections on the north side. These strike-slip faults formed a folded undulated structure in some parts, separating the horizontal positions of anomaly bearing conglomerate and sandstone sediments into numerous blocks.

The southern section of the main fault continued into a wide valley and the anomaly was closed-off by a covering of loose Quaternary sediments.

5. Comments on Possible Phosphate Origin and Genesis in Explored Area

Several observations can be made from the 4-year program of exploration for uranium in Mongolia during 2006–2009 in relation to various uranium target settings, in this case specifically phosphates. Related carbonate deposits, which are also developed in the landscape, are often well bedded, superficial, evaporate arid zone terrestrial freshwater limestone or calcareous cement that reflect the reaction of Ca^{2+} in neutral to alkaline groundwater with CO_2 to form carbonates. Such deposits

are seen in broad ephemeral depressions or within sand bodies filling older drainage channels. The calcium source would be from weathering of feldspar and especially from weathered basic volcanic rocks (Tertiary basalt sheets).

These can also be a source of phosphorus by the dissolution of apatite from basic volcanics under low pH settings. Other sources of phosphate are regionally from older Palaeozoic mafic oceanic basement rocks and Cretaceous shallow-water marine sediments that are currently eroding and redepositing in younger shallow and possibly terrestrial basin/lake settings. Younger marine sources of phosphate are also possible likely sources of uranium accumulation by incorporation of uranium in phosphate minerals in phosphate-rich mud, for example, in the Florida Banks phosphate deposits in the USA.

Phosphorus derived from mafic and basic magmatic sources is also likely to have associated higher levels of vanadium. This is important as the vanadium oxyanion is a significant oxyphilic element that readily complexes uranium in superficial environments as carnotite ($K_2(UO_2)_2(VO_4)_2 \cdot 3H_2O$) or tyuyamunite ($Ca(UO_2)_2(VO4)_2 \cdot nH_2O$). The phosphate oxyphilic complex equivalent of these in these settings is autunite ($Ca(UO_2)_2(PO4)_2 \cdot nH_2O$). The reaction is influenced by the pH of groundwater and solution ionic characteristics.

Exploration in the Sainshand–Zuunbayan area demonstrates that the superficial "uranium anomalies" that occur are related to the mobilization of the radiogenic daughter radium (^{226}Ra), radon (^{222}Rn), etc. from uranium enriched biotite bearing granites as found in conglomerate beds in the Sainshand formation (K_2ss). These granitic derived materials are probably the same source for uranium we drilled in at the Zuunbayan area (2008–2009) to the southwest. In considering reported interpretation of digitized U-Ra radiometric anomalism measured by the Soviets in their early work, it is most likely that it was considered related to Ra, Rn of recent origin and its radiogenic characteristics indicated significant radiogenic decay disequilibrium reflecting a recent derivation. In our exploration, we took a different view. We were looking at closed trap graben depression basins capped by younger sediments based on structural interpretations and not necessarily considering post basin fill cover, so we looked at Sainshand basin age sediment hosts in depressions, rather than the recent-age wind and stream water sediments that fill and cap the depression.

As to how rapidly the grabens are filling since the upper Cretaceous is not easy to determine as a tectonic activity is very frequent in this area. There are two types of sediment fill, slope wash, and scree of coarser oxidized material near the graben boundary fault margins related to uplift of the Palaeozoic horst units as seen in the wider district. This might have a range of ages. The other is the aeolian drift (barchan: mobile crescent-shaped sand dunes) and sheet wash sand fill typical of what is drilled in uranium exploration drill holes in graben depressions. This latter material is likely Holocene (Recent Neogene).

6. Environmental Issues

Outcrops in several Soviet exploration trenches encountered during these investigations had gamma radioactivity levels exceeding 1200 cps (Figure 9). Evidence for domestic animal grazing was encountered at each observation point. In some cases, nomadic settlements and winter shelters are present in the vicinity of highly radioactive outcrops (350–1000 cps). This radioactivity was not a result of excavation, but natural processes because the entire area is characterized by irregular, lens-like surface or near-surface concentrations of the trace elements as well as radioactivity (Figure 9).

Some of the anomalies needed to be characterized for environmental health and safety purposes, given sheep, goats, camels and other livestock traditionally bred in Mongolia are grazing and nomadic people are living on, or in their vicinity.

There was often better grass growth near the anomalies and observation points, which animals likely graze (Figure 10) possibly due to higher soil moisture toward the lower slopes coincident with heavy mineral accumulation, higher soil phosphate nutrient content, and precipitation in drainage trace. The animals are used as a source of milk and meat for human nutrition. The region is sparsely

populated, but the geologic characteristics of this location, and likely others, are questionable for long term human habitation. Roads also cut across the anomaly zones (Figure 9), although probably seldom traveled, but travelers could certainly inhale phosphate compounds, including radionuclides, along with dust.
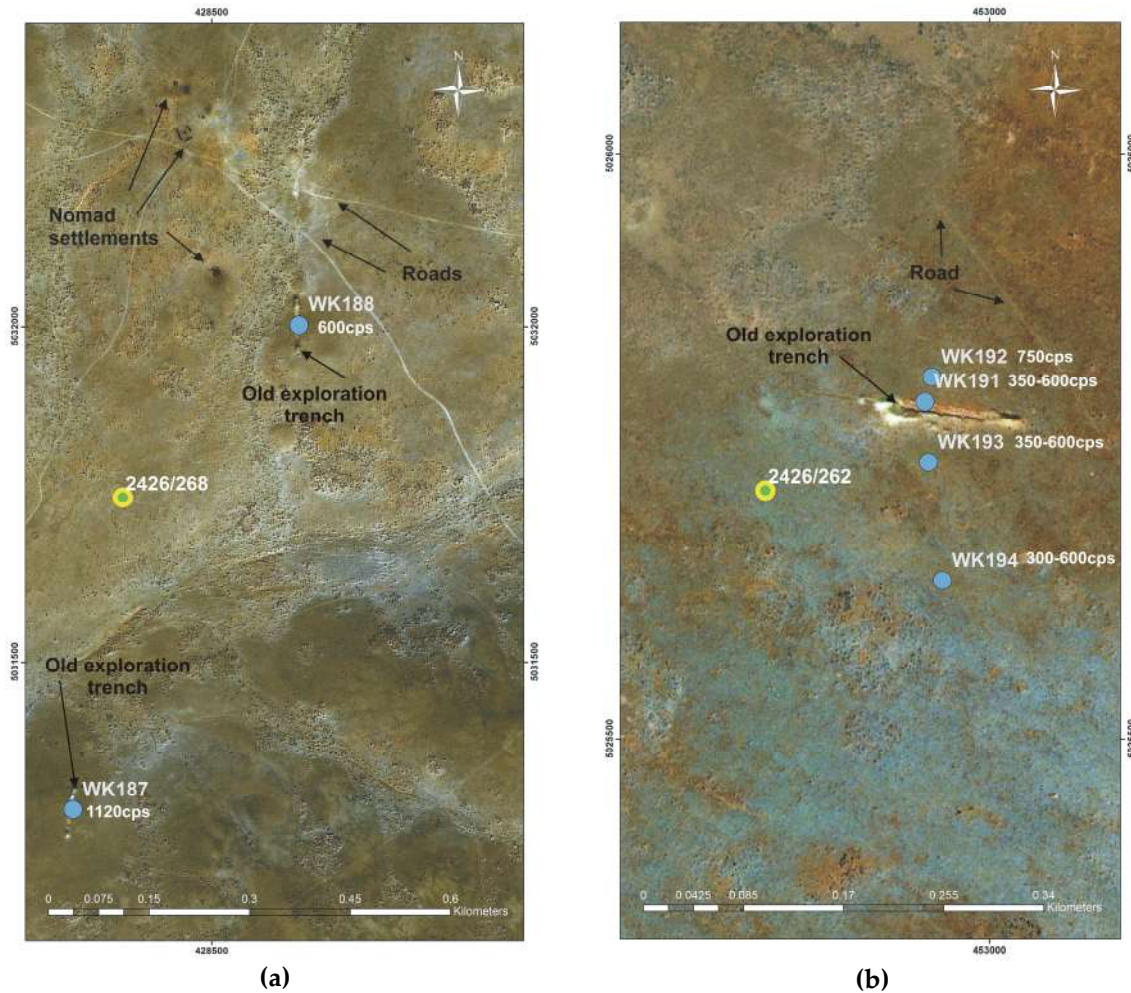

(a)   **(b)**

Figure 9. (**a**) Area of historic anomaly 2426/268 with recent observation points (blue dots) and nomadic settlement near sources of high radioactivity. Raster basis: SASPlanet ESRI ArcGIS Imagery; (**b**) area of historic anomaly 2426/262 with recent observation points (blue dots) and roads near sources of high radioactivity. Raster basis: SASPlanet ESRI Arc GIS Imagery.

Figure 10. Excavation trench near historic point 2426/262, with animal bones.

7. Conclusions

The objective of the 2011 exploration was to detect elevated concentrations of REE, U and related rare trace elements in radioactive phosphate-bearing anomalies. The outcome did not meet prospectivity expectations and we did not locate any REE or U bearing resources with economic potential. However, it did demonstrate the character of potential target settings and highlighted that similar settings are common in southeastern Mongolia.

The investigated anomalies were either superficial or very shallow (50–70 cm). It is possible in some cases that the concentrations of P and the elements of interest are elevated at greater depths as well. The grades of the analyzed elements were generally above typical average topsoil values based on literature sources [15–18]. In some instances, values were much higher than typical average values [16–18].

The published geological map of southeastern Mongolia corroborates the pattern described in this paper: Graben valleys built up of K_2ss with K_1dz outcrops at the contact with Quaternary sediments are a frequent occurrence and deserve attention during future investigations. The fault bound depressions act as traps for both heavy REE-enriched minerals derived from extensive erosion of a range of granite types and soluble species such as uranium, vanadium, phosphate, and carbonates. Uranium, leached from biotite rich granites can potentially be enriched in reduced carbon-rich sites in the depressions to form buried economic grade and size sediment hosted uranium deposits with ongoing basin hydrological flow through gravel and coarse sand beds, both shallowly and progressively to depth with ongoing basin depression and tectonic activity.

The economic potential is limited for most sites, but some may be indicative of areas that could also host blind mineralization at depth regionally within closed tectonic graben depressions.

Regional radiometric and geochemical investigations should be undertaken on a 2.5×2.5 km or 5×5 km grid to determine zones of anomalism. Wherever the concentrations of trace elements are found to be elevated, the grid density should be increased and testing repeated.

Also, an environmental survey should be conducted because of the relatively elevated sources of natural radioactivity exposed at and immediately below the land surface.

References

1. Hiatt, E.; Budd, D.A. Sedimentary phosphate formation in warm shallow waters: New insights into the palaeoceanography of the Permian Phosphoria Sea from analysis of phosphate oxygen isotopes. *Sediment. Geol.* **2001**, *145*, 119–133. [CrossRef]
2. Panda, N.K.; Rao, A.Y.; Kumar, K.R.; Mohanty, R.; Parihar, P.S. Anomalous REE concentration in carbonate-phosphate bearing phases from Narasimharajapuram area, Visakhapatnam district, Andhra Pradesh. *Curr. Sci.* **2015**, *109*, 860–862.
3. Emsbo, P.; McLaughlin, P.I.; Breit, G.N.; Du Bray, E.A.; Koenig, A.E. Rare earth elements in sedimentary phosphate deposits: Solution to the global REE crisis? *Gondwana Res.* **2015**, *27*, 776–785. [CrossRef]
4. Hassan, N.M.; Mansour, N.A.; Fayez-Hassan, M.; Sedqy, E. Assessment of natural radioactivity in fertilizers and phosphate ores in Egypt. *J. Taibah Univ. Sci.* **2016**, *10*, 296–306. [CrossRef]
5. Saleh, I.H.; Hafez, A.F.; Elanany, N.H.; Motaweh, H.A.; Naim, M.A. Radiological Study on Soils, Foodstuff and Fertilizers in the Alexandria Region, Egypt, Turkish. *J. Eng. Env. Sci.* **2007**, *31*, 9–17.

6. Llovet, X.; Melgarejo, J.C.; I Abat, L.T.; Villanova-De-Benavent, C.; Campeny, M.; Díaz-Acha, Y.; Amores-Casals, S.; Xu, J.; Proenza, J.A.; Ferre, E.T. Sandstone-Hosted Uranium Deposits as a Possible Source for Critical Elements: The Eureka Mine Case, Castell-Estaó, Catalonia. *Minerals* **2019**, *10*, 34. [CrossRef]

7. Díaz-Acha, Y.; Campeny, M.; Ferre, E.T.; Bosch, J.; Melgarejo, J.C.; Camprubí, A.; Villanova-De-Benavent, C.; Jorge-Villar, S.; Díaz-Ontiveros, I.; Fernández-Lluch, D.; et al. Critical Elements in Supergene Phosphates: The Example of the Weathering Profile at the Gavà Neolithic Mines, Catalonia, Spain. *Minerals* **2019**, *10*, 3. [CrossRef]

8. Gronen, L.; Sindern, S.; Katzmarzyk, J.L.; Bormann, U.; Hellmann, A.; Wotruba, H.; Meyer, F.M. Mineralogical and Chemical Characterization of Zr-REE-Nb Ores from Khalzan Buregtei (Mongolia)—Approaches to More Efficient Extraction of Rare Metals from Alkaline Granitoids. *Minerals* **2019**, *9*, 217. [CrossRef]

9. Boricki, D.B.; Zaichenko, V.P.; Pelmenev, M.D.; Dzaydok, V.P.; Ribnepv, G.V. *Report of Airborne Survey Results 1:25000–1:50000 Scale in East Gobi Area for 1979, MGSE 18, Irkutsk (MRAM 2426)*; Ministry of Geology USSR: Irkutsk, Russia, 1979.

10. Trusik, A.S.; Alekseev, L.M. *Geological Settings and Evaluation of Uranium Bearing Potential of East Mongolia, Geological Task MGSE-19 and VSEGEI-613 for 1979–1985 in 3 Volumes, Radiogeochemical Map*; Ministry of Geology USSR: Irkutsk, Russia, 1985.

11. Shmelev, Y.S.; Panev, V.; Gavrilov, Y.M.; Tataurov, V.D.; Chuvilin, V.A. *Results of Airborne Survey at Scale 1:200000 at Manlai Plateau*; Ministry of Geology USSR, "Zarubezgeologya", Mongolian Geological-Surveying Expedition, South Group: Sverdlovsk, Russia, 1983.

12. Troitskii, U.V.; Kaldishkin, V.A.; Kormilicin, V.S.; Kaldashkina, T.V. *Report on Prospecting-Exploration on Uranium in East Gobi Area for 1978–1980 (Geological task MGSE-15)*; Ministry of Geology USSR, "Zarubezgeologya", Mongolian Geological-Surveying Expedition: Sverdlovsk, Russia, 1981.

13. Jerden, J.J. Origin of Uranium Mineralization at Coles Hill Virginia (USA) and its Natural Attenuation within an Oxidizing Rock-Soil-Ground Water System. Ph.D. Thesis, Virginia Tech, Blacksburg, VA, USA, 2001.

14. Rutherford, N.F. *Review of Uranium Potential in Mongolia*; Mining Mongolia LLC and Gobi Coal and Energy, LLC: Ulaanbaatar, Mongolia, 2006; p. 99.

15. Agency for Toxic Substances and Disease Registry, ATSDR 1992. Available online: https://www.atsdr.cdc.gov/spl/resources/1992_atsdr_substance_priority_list.html (accessed on 25 December 2019).

16. Salminen, R. *Geochemical Atlas of Europe, Part 1: Background Information, Methodology and Maps*; Geological Survey of Finland: Espoo, Finland, 2005; ISBN 951-690-913-2.

17. De Vos, W.; Tarvainen, T. *Geochemical Atlas of Europe, Part 2: Interpretation of Geochemical Maps, Additional Tables, Figures, Maps and Related Publications*; Geological Survey of Finland: Espoo, Finland, 2005; ISBN 951-690-960-4.

18. *Abudance of Elements in the Earth's Crust and in the Sea, CRC Handbook of Chemistry and Physics*; CRC: Boca Raton, FL, USA, 2016–2017; pp. 14–17.